Performance Analysis of Piezoelectric Multi-cantilever Array System with Different Mass Configurations

Fahmidul Huq Syed[1], Li Wah Thong[1]*, Yee Kit Chan[1]

[1] *Multimedia University, Faculty of Engineering and Technology*
Jalan Ayer Keroh Lama, Melaka, 75450, MALAYSIA

*Corresponding Author: lwthong@mmu.edu.my
DOI: https://doi.org/10.30880/ijie.2024.16.03.012

Article Info	Abstract
	This paper presents a piezoelectric array harvester using five array beams with piezo patches on their fixed ends and tip masses situated on various locations on the beams. The simulation-based study is conducted in COMSOL Multiphysics within a range of 0-40 Hz to inspect and evaluate the bandwidth frequency of the voltage output. Three different categories A, B & C have been studied including three different materials, tungsten, steel, and aluminum used on the array beams and the tip mass to investigate the effect of the weight and the location of the tip mass on the beam. Additionally, twenty sub-categories of configuration of the tip mass have been presented and evaluated in the paper. The collected data from different arrangements of the block masses and the use of different materials helped conclude the correlation among the location, weight of the tip mass, the magnitude of outcome and resonant frequencies. The paper identifies potential arrangements of multi-cantilever array system to broaden the bandwidth frequency.

1. Introduction

The primary trends in the development of electronic devices right now are miniaturization, multifunctionality, portability, flexibility, considerable processing capabilities, and efficient low-power networking [1]. It is possible to supply many electrical devices with long-lasting power by harnessing ambient energy sources such mechanical vibrations, heat, fluid movements, electromagnetic radiation (light and radio waves), and biological energies. Wireless sensor networks, portable electronics, and wearable and implanted biomedical devices are some of these gadgets. These gadgets have often been powered by electrochemical batteries. The cost of recharging or replacing batteries is increased by the fact that they have a finite lifespan that is frequently shorter than that of the devices themselves. In the case of biomedical equipment, changing the batteries necessitates extra procedures, putting patients at risk for infection and other problems while also costing hospitals money. Additionally, batteries are big and add a lot to the size and weight of electronic gadgets, which prevents their miniaturization. A lot of research and development has been put into enhancing energy harvesting technologies as self-powering options for a variety of wireless electronic devices in response to these difficulties [2]

Although we are surrounded by ambient sources of energy to harvest from, one of the easiest and commonest sources is vibration, therefore over the years it has taken a hike of interest among the researchers for well listed reasons [3][4]. The vibration found in our surroundings can easily be transformed into electrical output via electromagnetic, electrostatic, or piezoelectric method [5]. Albeit the generated electrical output using the amendatory vibration is not scalable enough to power big devices, they are quite sufficient to power electronic devices that require minimum electrical inputs [6]. Although these harvesters produce clean energy and with a high resonant peak, the limitations occur at their shrink bandwidth [7]. Hence, the implementation arrays are a way of creating a broadband harvesting system to satisfy a constant output within a range of frequencies showing

multiple resonant frequencies instead of one. Array harvesters are not a new phenomenon that has been studied or implemented. Over the years, to broaden the natural frequency, many implementations have been made by many researchers. External magnets have been used to enhance the power density [8], frequency tuning has been applied to broaden the bandwidth with sliding masses [9]. Different shapes of harvesters have been tested to attain optimization [10], similarly graded piezoelectric beams have been used for further development in the field [11].

This paper presents how the location of the tip mass reflects on the outcome of the natural broadband frequency. COMSOL Multiphysics have been used to evaluate and achieve the voltage and electrical power outcome within a range of 40 Hz. This linear array approach takes the finding of the effect of location of the mass impacting the outcome based on the results achieved on single cantilever beams in previous studies [12] are considered.

2. Design of the System

2.1 Vibration Energy Harvesting Method

Electromagnetic, electrostatic, and piezoelectric are the three fundamental choices when it comes to Vibration energy harvesting [13]. Among these three, piezoelectric method is known for its accuracy, precision and coverage over a large range of natural frequency [14][15]. Hence its use can lately be seen in military as well. The simplicity of the design and fabrication, as well as the efficiency of conversion in real time dictates piezoelectric method over the other two.

2.2 Analytical Method

The analytical modelling of a multi-cantilever beamed piezoelectric energy harvester can be derived using Euler-Bernoulli's equation and can be expressed as the following,

$$-\frac{\partial^2 M(x,t)}{\partial x^2} + c_s I \frac{\partial^5 z_{rel}(x,t)}{\partial x^4 \partial t} + c_a \frac{\partial z_{rel}(x,t)}{\partial t} + m \frac{\partial^2 z_{rel}(x,t)}{\partial t^2} = -(m + m_t)\frac{\partial^2 z_b(x,t)}{\partial t^2} \tag{1}$$

In equation 1, $M(x,t)$ quotes the bending moment applied on the harvester, z_{rel} is the transverse deflection, the second moment of inertia is represented by I, the strain damping is represented by c_s, the viscous damping or air is presented by c_a, the mass of the harvester is m and m_t is the tip mass. The base excitation is $z_b(x,t)$.

$$\frac{\partial^2 M(x,t)}{\partial x^2} + m \frac{\partial^2 z(x,t)}{\partial t^2} = f_o(x,t) \tag{2}$$

Substituting the undamped force in equation 1 leads us to equation 2, where $f_o(x,t)$ signifies as the inertia force caused by the base excitation. Since, free vibration has been used for natural frequency, substituting $f_o(x,t)= 0$ leads us to the following,

$$\frac{\partial^2 M(x,t)}{\partial x^2} + m \frac{\partial^2 z(x,t)}{\partial t^2} = 0 \tag{3}$$

Equation 4 expresses the mass of the harvester, m. In this circumstance, the density of the substrate layer material and piezoelectric material is expressed as p_s and p_p, h_s and h_p signifies the thickness of the substrate material and the piezoelectrical layer. L is the length of the cantilever and L_p is the length of the piezoelectric layer and b stands for width of the cantilever.

$$m = b (\rho_s h_s L + \rho_p h_p L_p) \tag{4}$$

The voltage, resistance and power can be expressed in the three following equations,

$$v = \sum_{n=1}^{N} \left(\frac{\frac{E_p}{\varepsilon}(\frac{2a_{in}k_{31}h_p}{k_2})^2}{[\frac{\omega_n^2}{\omega R c_p} - \omega\left(\frac{1}{R c_p} + 2\omega_n\zeta\right)]^2 + [\omega_n^2(1 + k_{31}^2) + \frac{2\omega_n\zeta}{R c_p} - \omega^2]} \right)^{0.5} \tag{5}$$

$$R = \frac{1}{c_p \omega_n} \frac{2\zeta}{\sqrt{4\zeta^2 + k_{31}^4}} \tag{6}$$

$$Power = v \left(\frac{2k^2}{\frac{\pi}{2} + Rc_p\omega_n} + \frac{\frac{\pi}{2} + Rc_p\omega_n}{\alpha_2 R} \right) \tag{7}$$

In the equations presented above, ω_n is the natural frequency. The amplitude of the base acceleration is presented by *ain*. K_{31} and ζ is the coupling coefficient and the damping ratio. The dielectric constant is represented by ε. The expression c_p is the capacitance and can be expressed as,

$$c_p = \frac{2\varepsilon b L_p}{h_p} \tag{8}$$

The simulation ran in COMSOL Multiphysics on a multi-cantilever basis piezoelectric energy harvester can be validated by this analytical model presented.

2.3 Parameters and Simulation

COMSOL Multiphysics was used to design an array of beams holding a mass block on one end and a piezo patch adjusted on the fixed end of the beam. Figure 1 represents the visual illustration of the 3D model drawn in COMSOL Multiphysics of the multi cantilever beam. The blue arrow in the figure identifies the piezo patches attached to each beam on one end and the tip masses placed on the other end of each beam respectively. The dimensions of each structure have been mentioned in Table 1. Table 2 showcases the properties of the materials used for the study.
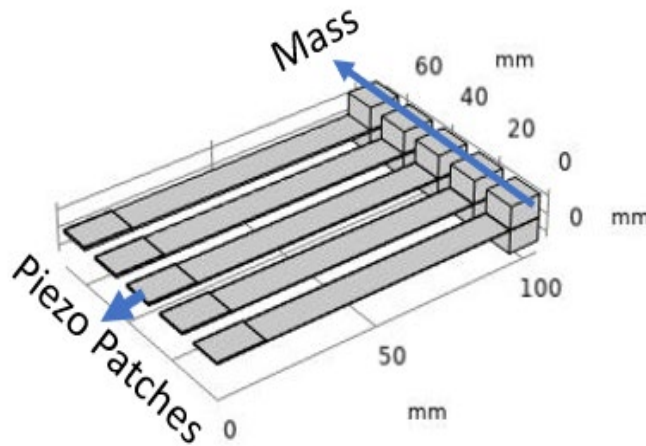

Fig. 1 *Piezoelectric array harvester*

The dimension of each structure is mentioned in Table 1 and Table 2 showcase the properties of the materials used for the study. These exact dimensions and model was created for the study in accordance with the study conducted by Sallam A. Kouritem[16] where the angle of the tip masses were controlled in an inclination to improve the output. An array of five identical beams, blocks and piezo patches was used. To establish a justification of the results, the same model was designed keeping all the parameters identical to the aforementioned study. Three different materials were used for the blocks and the beam while the piezo material remained the same throughout the whole process. The range of frequency was kept from 0 to 40 Hz. Each array beam had its eigenfrequency as shown in Figure 2. The positioning of the blocks was categorized into three main domains as shown in Figure 3. Each of these domains have been subcategorized by repositing one array block at a different location than the rest of the blocks to monitor the changes in the output.

To simulate the applied vibration, the array of beams was put through a base excitation. The motive of using three different materials for the array beam and the tip mass was to inspect the effect of different weights in a broadband system. Tungsten, among the three is the heaviest material and Aluminium is the lightest material.

The blocks were plotted in three different locations of the array beam. Although it is noticed in Figure 3 (A), (B) and (C), on each array harvester, the tip masses were stagnant at the same distance, in the subcategories on the same array harvester the tip masses were plotted at different distances on each array beam. Under these three main categories (A, B and C), we studied several subcategories by placing one of the tip masses on a single beam array by placing it on a different location of the beam compared to the rest of the tip mass's location on their respective beams as shown in Figure 4.

Table 1 *Geometrical parameters*

Category	mm
Length of piezo patch	15
Width of piezo patch	10
Thickness of piezo patch	0.3
Length of beam	95
Width of beam	50
Thickness of beam	0.3
Length of block (mass)	10
Width of block (mass)	10
Thickness of block (mass)	13.1

Table 2 *Material properties*

Material	Properties	Value
PVDF (Piezoelectric)	Young's Modulus (Pa)	3.8×10^9
	Density (kg/m³)	1780
	Poisson's ratio	0.33
Steel	Young's Modulus (Pa)	200×10^9
	Density (kg/m³)	7850
	Poisson's ratio	0.30
Tungsten	Young's Modulus (Pa)	411×10^9
	Density (kg/m³)	19350
	Poisson's ratio	0.28
Aluminium	Young's Modulus (Pa)	70×10^9
	Density (kg/m³)	2700
	Poisson's ratio	0.33

5.8379 Hz

8.8242 Hz

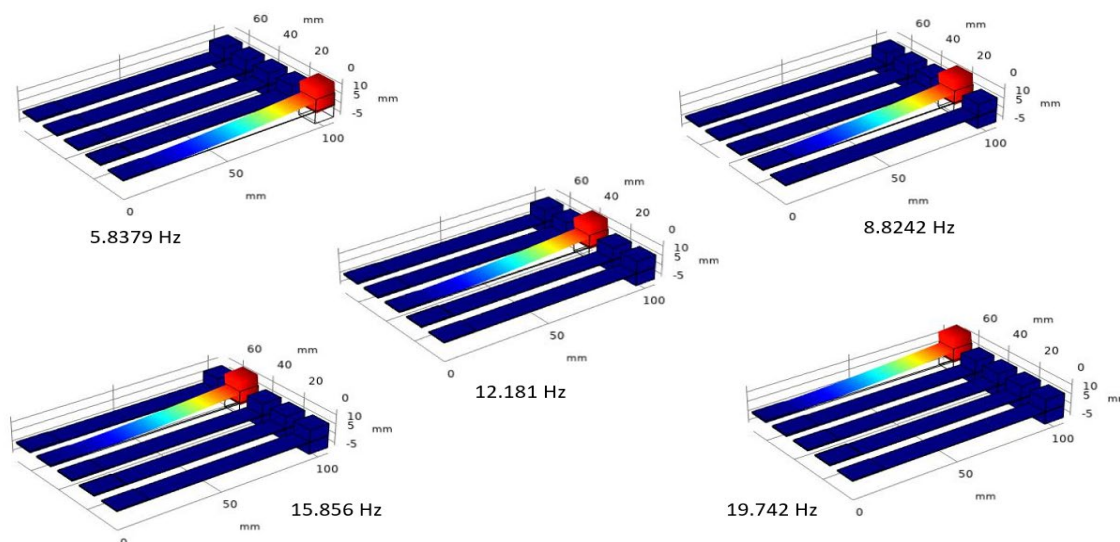12.181 Hz

15.856 Hz

19.742 Hz

Fig. 2 *Eigenfrequency of each array beam*
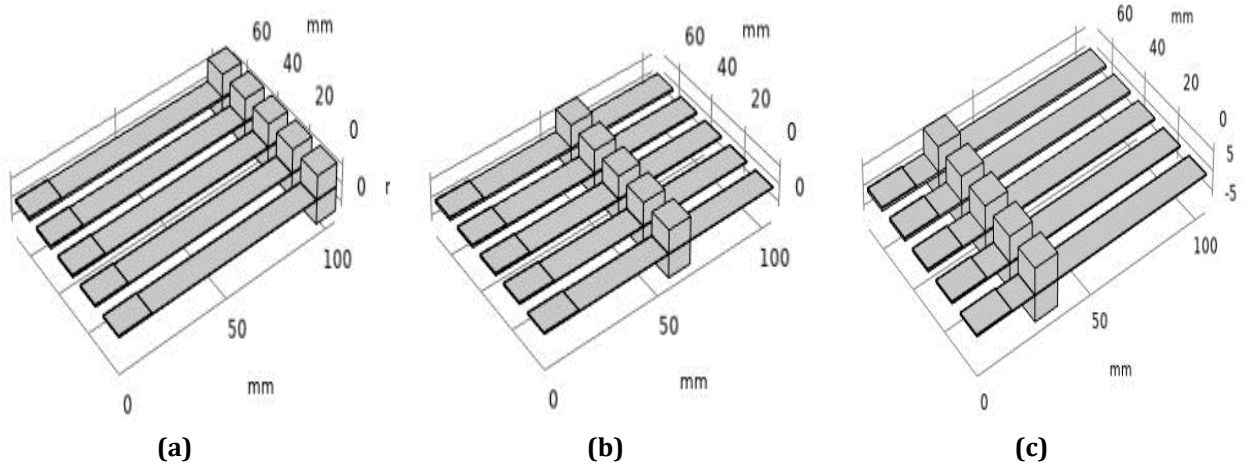
Fig. 3 *Configurations A, B and C of the array based on the tip mass location*

Table 3 *Location of tip mass*

Category	Location on the array beam (mm)
A	95
B	55
C	25

Table 4 - *Parameter of subcategory configurations*

Subcategory	Beam 1 (mm)	Beam 2 (mm)	Beam 3 (mm)	Beam 4 (mm)	Beam 5 (mm)
A1	55	95	95	95	95
A2	95	55	95	95	95
A3	95	95	55	95	95
A4	95	95	95	55	95
A5	95	95	95	95	55
B1	95	55	55	55	55
B2	55	95	55	55	55
B3	55	55	95	55	55
B4	55	55	55	95	55
B5	55	55	55	55	95
C1	95	25	25	25	25
C2	25	95	25	25	25
C3	25	25	95	25	25
C4	25	25	25	95	25
C5	25	25	25	25	95
C6	55	25	25	25	25
C7	25	55	25	25	25
C8	25	25	55	25	25
C9	25	25	25	55	25
C10	25	25	25	25	55

A1   A2   A3

A4   A5

(a)

B1   B2   B3

B4   B5

(b)

C1   C2   C3

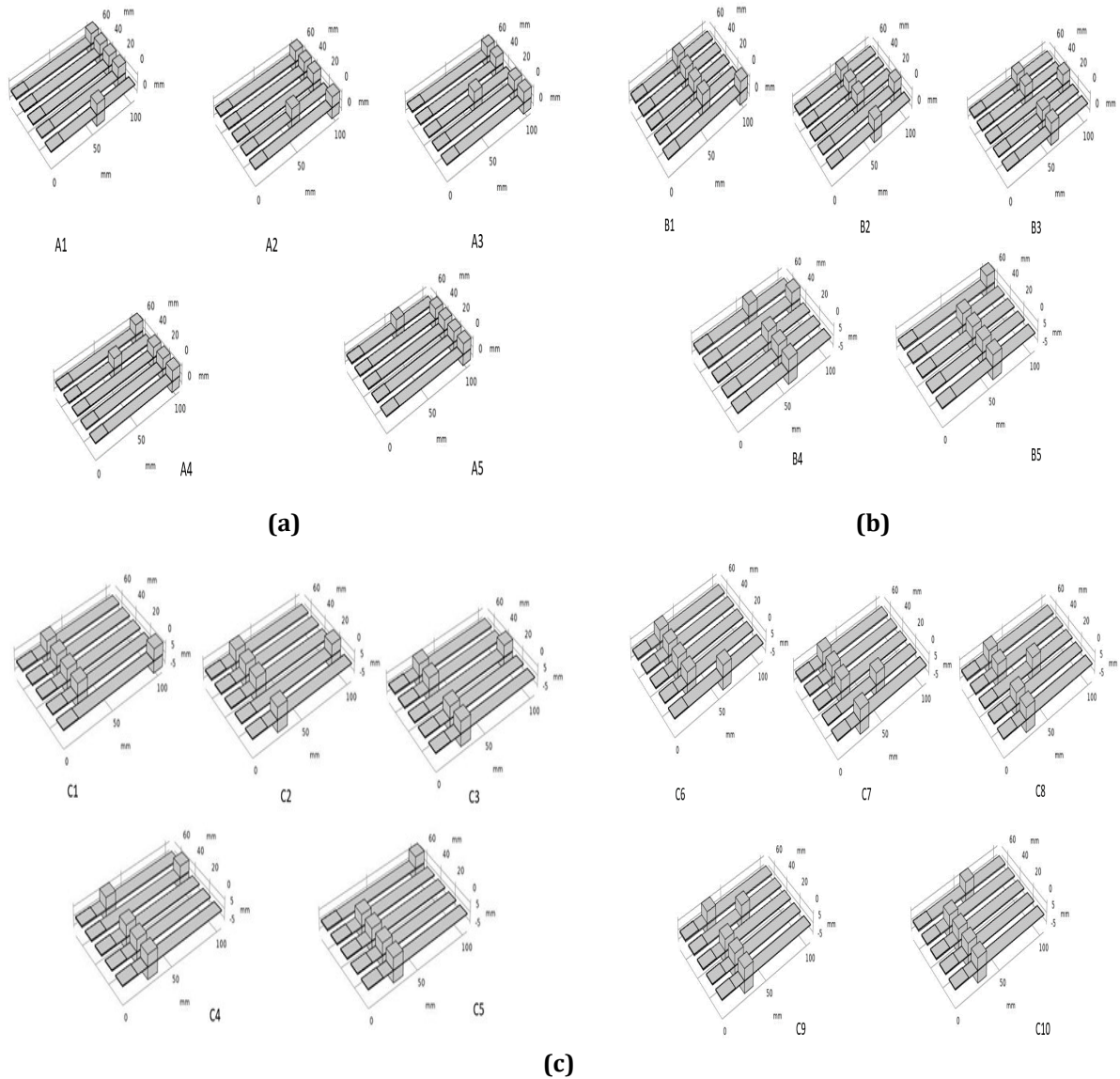C4   C5

C6   C7   C8

C9   C10

(c)

Fig. 4 *(a) subcategories of A; (b) subcategories of B; (c) subcategories of C*

3. Results

The simulation of all the cases produced a voltage and electrical power graph for each configuration. In this paper, only the voltage output has been presented and discussed as a medium of comparison since the electrical outputs are minimal and follow the same graph as voltage.

3.1 Category A and Subcategories

Case A5 displayed the highest voltage outcome of 10V at 35Hz. However, among all the other cases in category A, A5 is the most inconsistent despite producing the maximum output. The rest of the subcategories displayed a stable outcome within the range of 1V-2.5V. A1 and A2 are the only two cases where only 4 peaks have emerged within the frequency range. The major problem of piezoelectricity is a single maximum resonance instead of a stable resonance covering a continuity in the frequency range. However, in this category, A1 has been the only subdivision where a stable outcome has emerged for a repetitive range in the frequency. A1 displayed a minimum 0.2V output from 8Hz-14Hz. Although the voltage output is not of high magnitude, it displays the potential of overcoming the problem with piezometry as aforementioned.

As displayed in figure 5, the resonant frequencies in all the cases are inconsistent, the highest peak in all the cases have seen to be evidently larger than the rest of the peaks. In A4, every following resonant frequency has topped the previous one, the first resonant frequency at 6Hz showing the lowest peak as the fifth resonant frequency displayed the highest peak at 29Hz, surpassing the double of the magnitude of the first voltage outcome.

The orientation of the tip masses in category A proved the potential of producing voltages of high magnitude (10V in A5), as well as having a consistent output in several frequencies (In A1).

The voltage graphs presented in figure 5 also indicate the similarity in the voltage spike from A to A4. Although A1 and A2 did not display all their peaks within the range of study, the existing curves under the blue hints to the cases sharing similarities in their output.

3.2 Category B and Subcategories

Figure 6 highlighted the voltage output in category B. While the graphs produced by B to B4 looked similar to the voltage graph produced by A5 (shown in figure 5), B5 generated a voltage curve nearly similar to the voltage graphs generated by case A to A4 (Shown in figure 5). However, the subtle difference between B5 and the subcategory of A is the peak output. Most of the peak resonance occurred in the third or fourth voltage spike for case A, however, in B5, the second spike was seen to be of highest magnitude. B5 showcased the lowest voltage magnitudes, but it produced peak frequencies in a much closer range, proving itself a more stable configuration from the rest. B5 produced a maximum output of 1.9V. The lowest resonant outcome at 11Hz was 0.5V.

However, the rest of the configurations in category B produced their maximum outcome on their last peak within the frequency range, resulting in over 10Hz in each case. The other peaks that emerged in these subdivisions could barely produce 20% of the highest peak.

Additionally, even though category B produced graphs similar to category A, it failed to display even one single case showcasing stability in the bandwidth of the output. To compare both these categories (A and B), A performs more superior than B since the subcategories in A have delivered a range of different values, each suitable for different applications or devices.

3.3 Category C and Subcategories

Since category C had the maximum number of subcategories, the voltage graphs attained in this part are very different from the previous two categories. First and foremost, none of the subcategories could not display five peaks within the studied range. Hence, it confirmed that the arrangement of the multi-cantilever with their tip masses performs in a frequency range higher than 40Hz.

C10 delivered similar output to category B and A5, the last resonant frequency peaking over 10V at 35Hz. The rest of the subcategories showed peak voltage output within the range of 1V-2.5V in different cases.

Unlike category B, category C showed multiple cases producing a wider frequency bandwidth. Although, none of the cases could present all five peaks within the frequency range, most of them showed moderately wide bandwidth frequency. For instance, C1 showed a very gradual inclination on its second peak, causing the bandwidth to be wider although the output is of a lower magnitude. A similar graph was seen in C6 too. But the first peak of C6 had a wider bandwidth than the first peak in C1.

Similarly, C3, C4, C5, C8, C9 showcased bandwidth frequencies that are considerably and evidently wider than the results attained in category A and B. Subcategories of C displayed values that can offer more variety to numerous devices of applications compared to the combination of results found in category A and B.
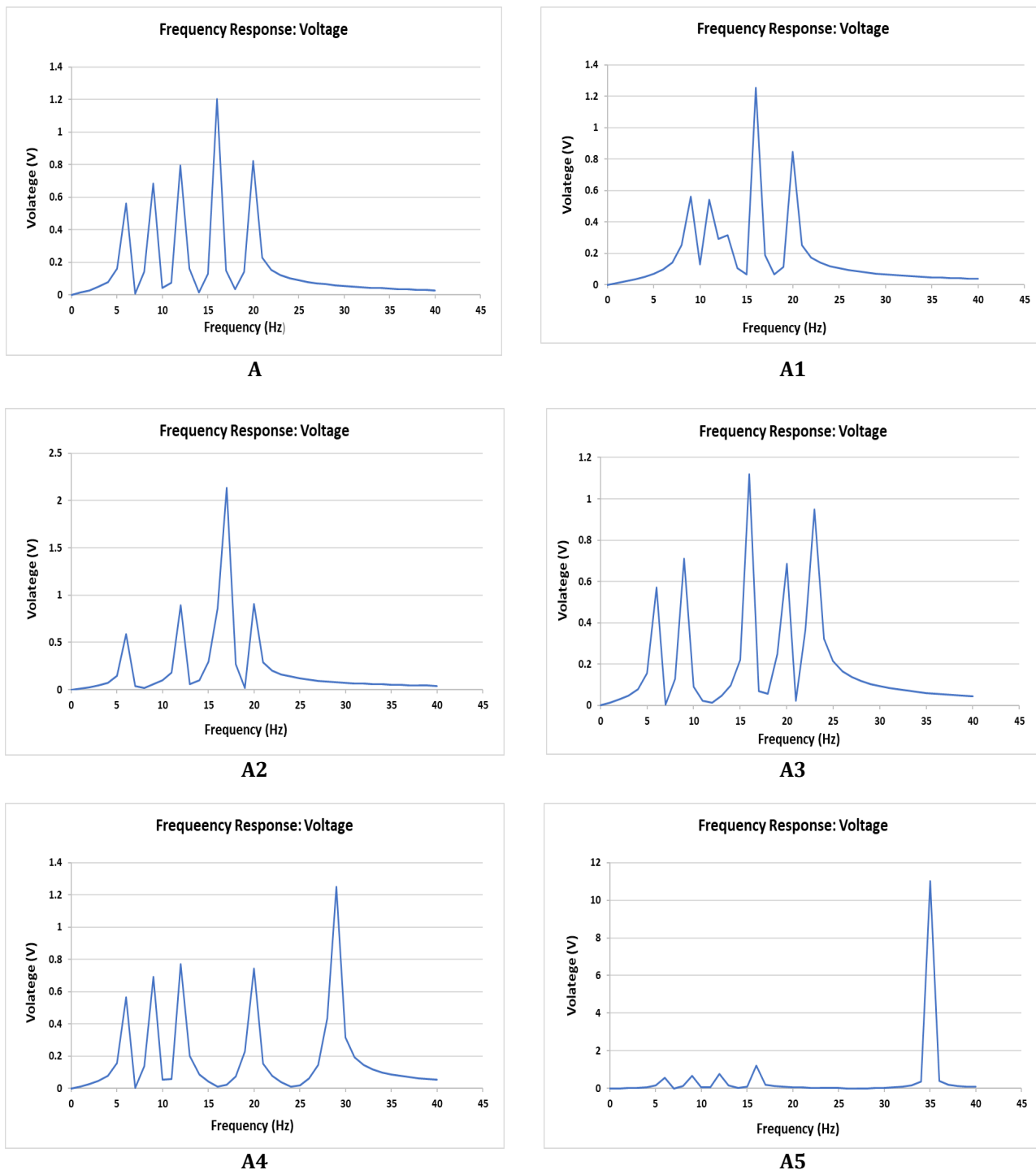
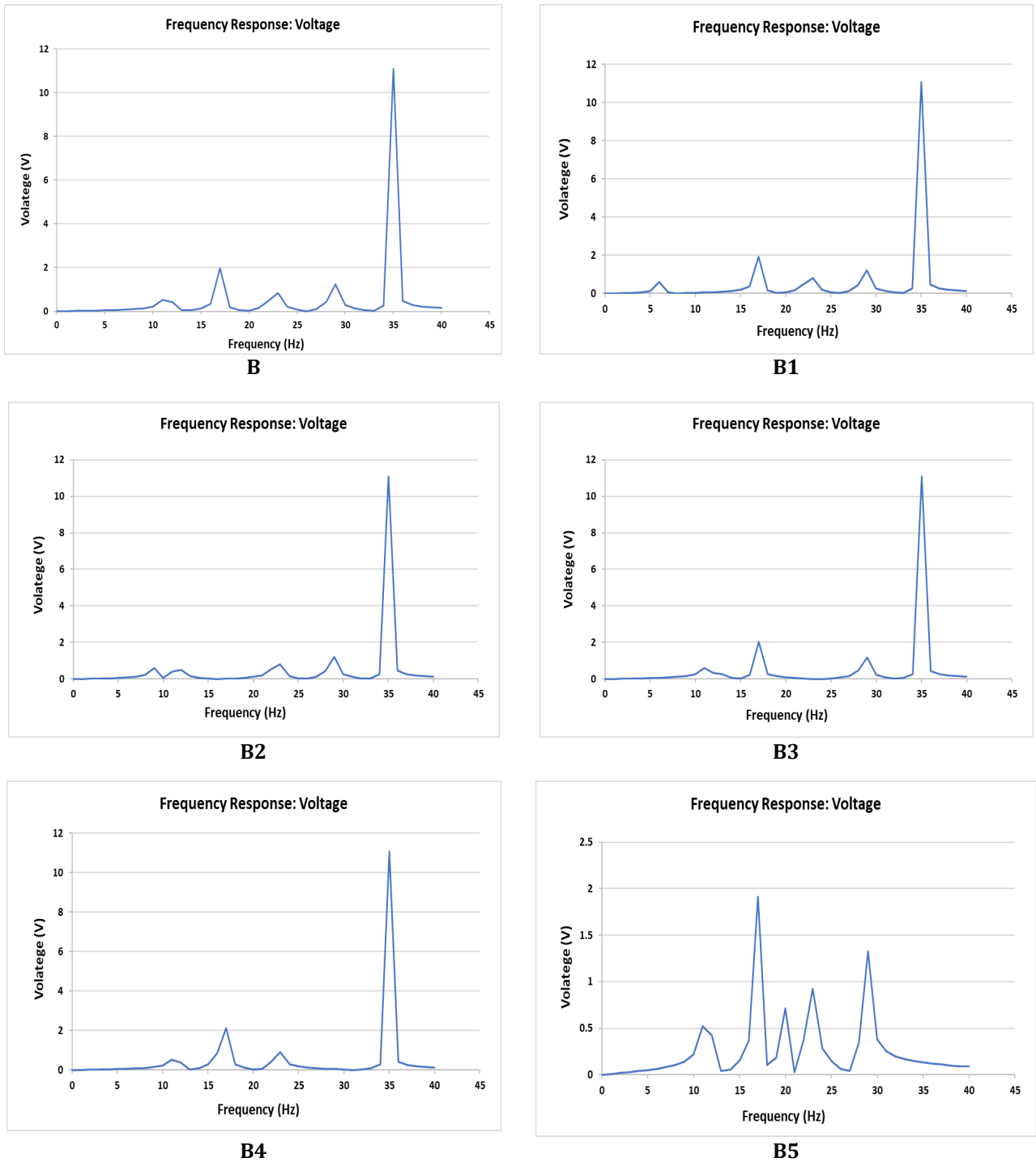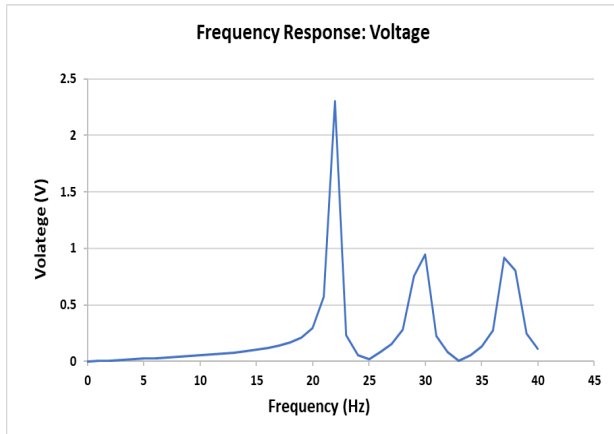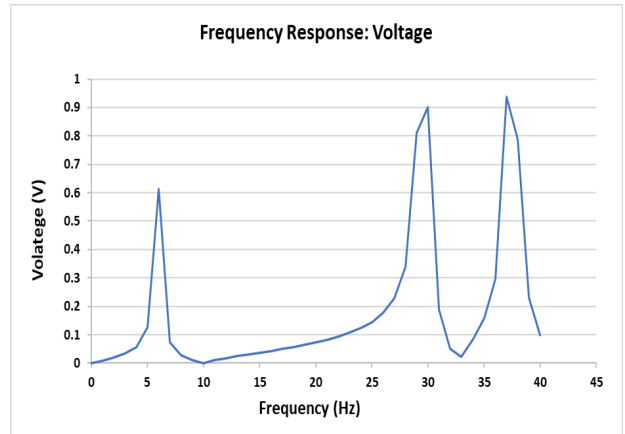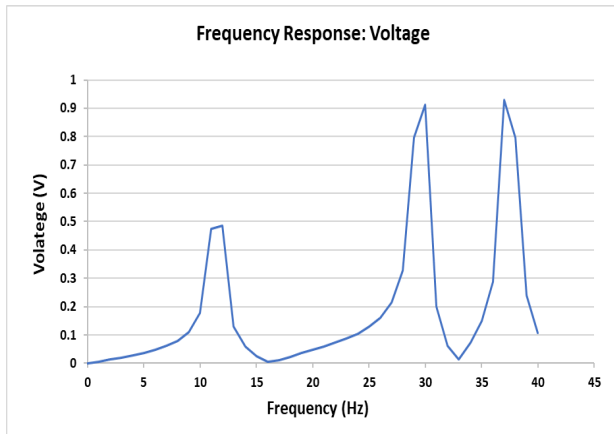**Fig. 5** *Voltage output of category A and its subcategories*

Fig. 6 *Voltage output of category B and its subcategories*
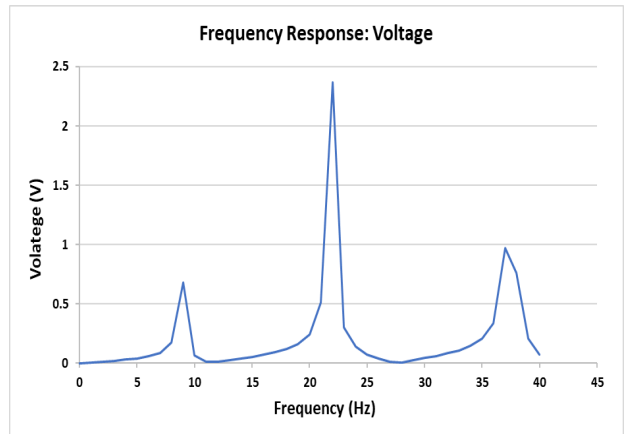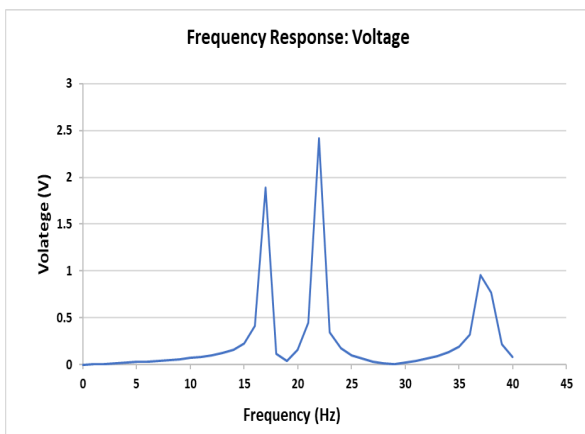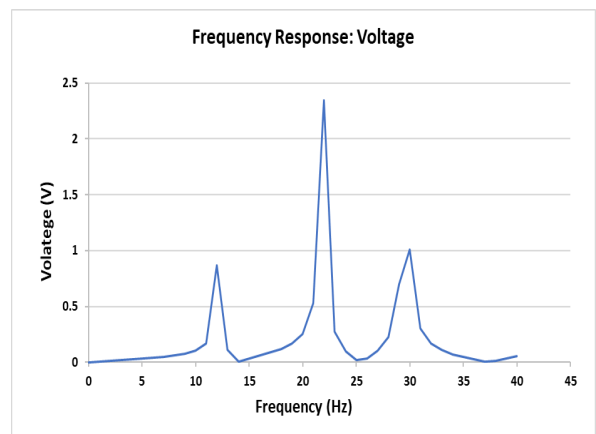
C

C1

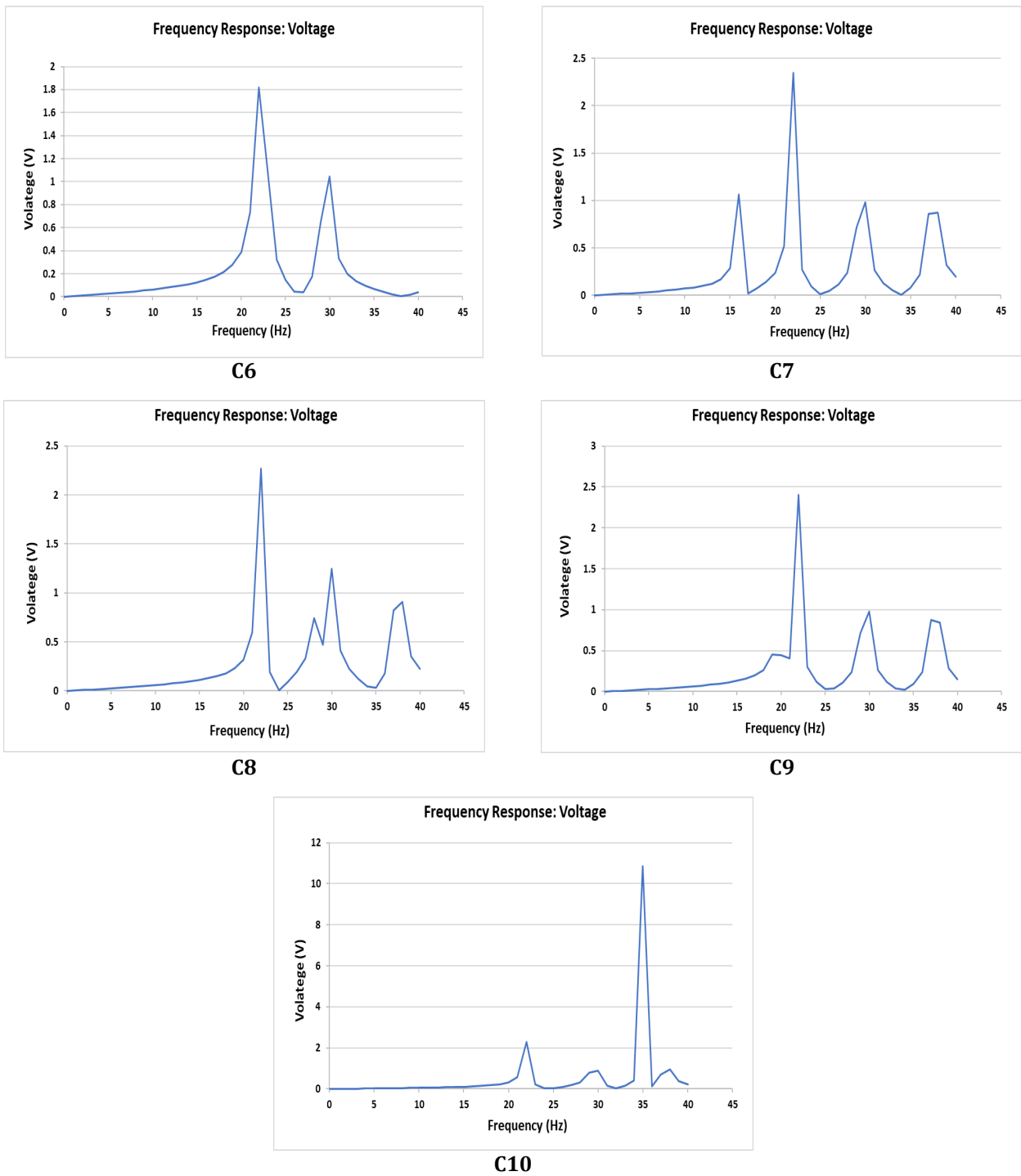
C2

C3

C4

C5

C6

C7

C8

C9

C10

Fig. 7 *Voltage output of category C and its subcategories*

3.4 Different Array Beam and Tip Mass Material

Three different materials for the array beam and the tip mass (Table 2) were used. The change in the materials showed different results with the same array configuration. Figure 8, 9 and 10 portrays the combined results of each material for Category A, B and C.
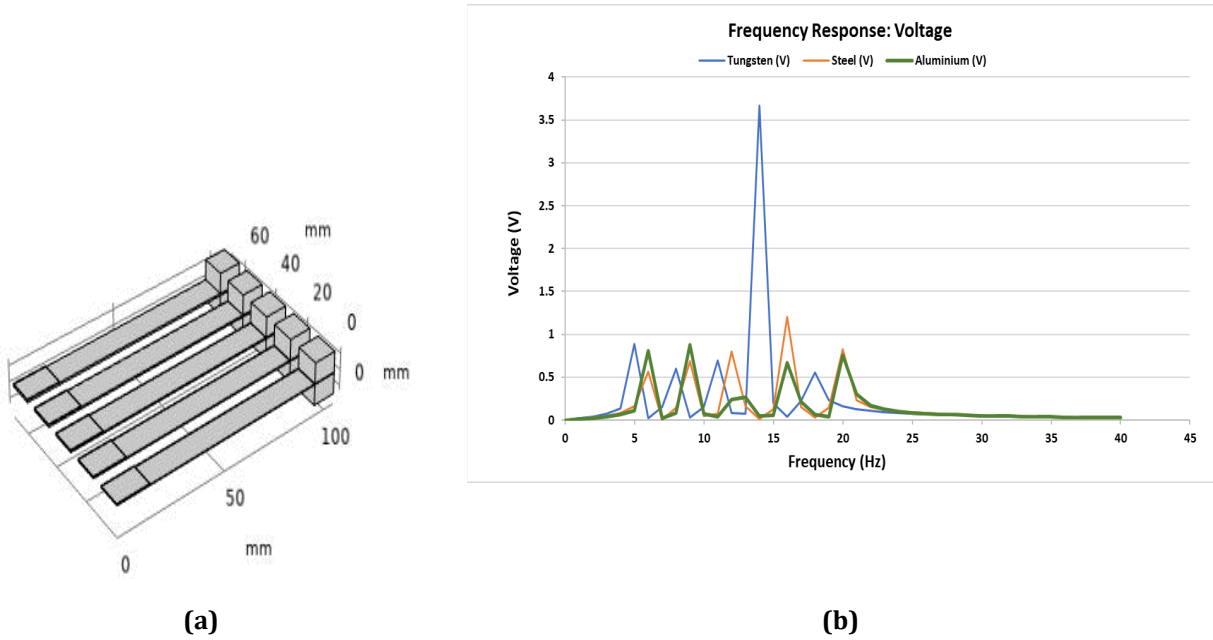
Fig. 8 *(a) Category A configuration (b) Voltage outcome by using different materials for category A*

All the materials display a consistent array of peaks within the range of 23 Hz. Tungsten displays a maximum peak of 3.66 V at 14 Hz while the rest of the peaks of tungsten is below 1 V. 1.20 V is the maximum peak achieved by Steel at 16 Hz and 0.87 V is the highest output voltage of aluminium at 9 Hz.
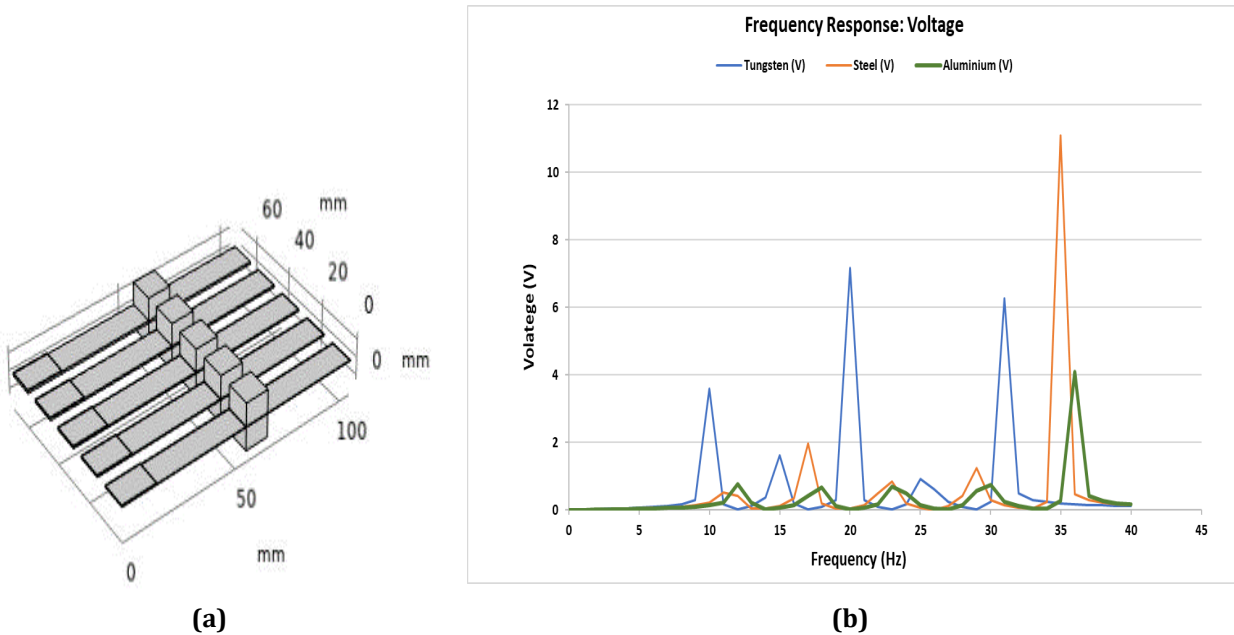

Fig. 9 *(a) Category B configuration; (b) Voltage outcome by using different materials for category B*

While category A shows a repetitive array of peaks within 23 Hz, category B display peaks of higher value but spread further apart within a range of 40 Hz. However, tungsten shows a regular array of resonance with five peaks. The maximum voltage output achieved by tungsten is 7.18 V at 20 Hz. Steel produces the highest voltage output of 11.1 V at 35 Hz, with a rapid inclined peak from producing an output of 0.25 V at 34 Hz and a stiff decline as it gives an output of only 0.47 V at 36 Hz. Aluminium showcases an output of 4.09 V at 36 Hz, while the rest of the peaks achieved by aluminium rests below 0.8 V.
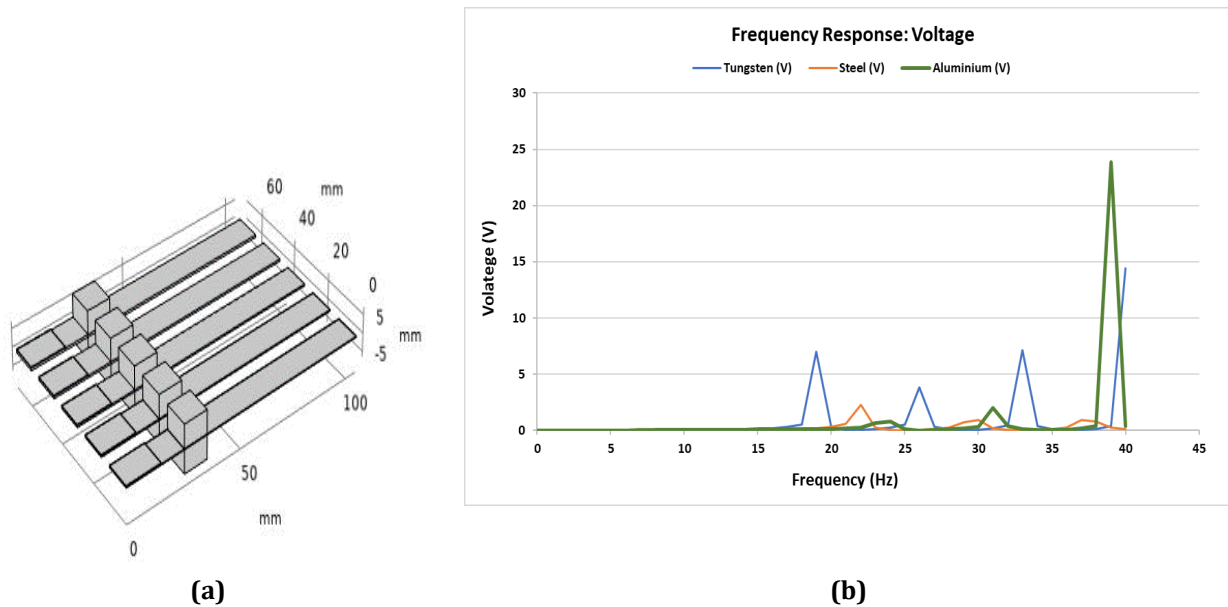
(a)   **(b)**

Fig. 10 *(a) Category B configuration; (b) Voltage outcome by using different materials for category C*

The first peak of tungsten in category C is noticed at 19 Hz, producing an output of 6.99 V. Aluminium displays a sudden peak at 39 Hz jumping from an output voltage of 0.4 at 38 Hz to producing 23.87 V. 2.30 V has been produced by steel at 23 Hz which is the highest voltage output for steel.

4. Discussion

The motive of using an array of beams is to produce a decent bandwidth to maintain a flow of power to contribute to running devices that require low input of power. Over the years, researchers have implemented many methods to enhance the results, both value wise [7] and by trying to improve the bandwidth [17]. In this paper, our approach is to advocate for the best outcome to improve the bandwidth of the system. We have discussed 23 cases by situating the tip masses on different locations on the array beams. We have used three different cases by changing the material of the array beams and the tip masses to inspect and evaluate the differences. Category A and its subcategories have produced very promising results within our range of frequencies. We have witnessed five nearly similar peaks in every case below the range of 40 Hz, although the voltage outputs are not as skyrocketing as category B, nevertheless, it showed a stable outcome within the range. Category C showed the least peaks within the studied range (40Hz), hinting that the multi-cantilever performs within a range higher than 40Hz to display all five peaks.

Additionally, the data obtained from category C portrayed the maximum number of sub-categories showcasing broader bandwidth frequencies. The pattern in all three categories was that category A resonated within the lowest frequency among all three categories. All peaks were visible within 20Hz. Category B showcased all its peaks at a higher frequency compared to category A, the last peak resonant frequency among all five peaks were mostly noticed at 35Hz (Except for B5). The data from category C did not show all five peaks in any of its cases, a maximum of 4 peaks were seen C4, C9 and C10. The data from category C clarified its range of frequency was higher than our range of study (40 Hz).

As we evaluated the differences among the results of category A,B and C upon using tungsten, steel and aluminium (Figure 8-10), we noticed the behavioural pattern of the materials based on their weight and their location on the beam as concluded by [12]. Heavier material such as tungsten displayed higher and more consistent peaks at lower frequencies. Lighter materials displayed lower outcomes at higher frequencies. Also as mentioned in [12], further the tip mass is located on the beam, the resonant frequency is lower which is evident in Figure 8, 9 and 1. Let us take tungsten for example, in category A, all five peaks of tungsten have appeared within 20 Hz where the tip masses are situated at 95mm on the array beams. As the tip masses were located closer on the array beam in category B, the resonant peaks appeared further at 10 Hz till 31 Hz. In category C where the tip masses were placed closest to the fixed end and the piezo patch, the first peak appeared at 19 Hz and the fourth peak is beyond 40 Hz. This establishes and allows freedom of using any configuration of array based on the requirement of any device or application. If a device, application, or system is required to resonate in a range of 10-30 Hz, then we know category B is a better option. If the system requires resonating within a range of 20 Hz, then category A outperforms the rest.

5. Conclusion

This paper approaches a linear method to broaden the bandwidth frequency on array harvesters and successfully proposes ways of enhancement on results and choices of substitutional arrangement based on the need of any particular system. Narrow bandwidth being a consistent problem in the area of piezoelectricity, this paper studies a fundamental way of running a scrutiny based on various arrangements of the block masses in an array system, without any involvement of any additional phenomena to maximize the output. Category C delivered multiple orientations of the system to provide a wider bandwidth frequency. However, these potential results can be further enhanced by using techniques like frequency tuning. Additionally, heavier materials produce higher magnitude of outcome at lower frequencies. A tip mass located further on the beam shows lower resonant frequencies. This creates an opportunity to develop devices or systems that require higher outputs at lower frequencies as well as to develop a device that may require outputs at a higher range of frequency.

Acknowledgement

Conflict of Interest

Authors declare that there is no conflict of interests regarding the publication of the paper.

Author Contribution

*The authors confirm contribution to the paper as follows: **study conception and design:** Fahmidul Syed Huq, Li Wah Thong; **data collection:** Fahmidul Syed Huq; **analysis and interpretation of results:** Fahmidul Syed Huq, Li Wah Thong; **draft manuscript preparation:** Fahmidul Syed Huq, Li Wah Thong, Chan Yee Kit. All authors reviewed the results and approved the final version of the manuscript.*

References

[1] H. Deng *et al.*, "Poly-stable energy harvesting based on synergetic multistable vibration," *Commun. Phys.*, vol. 2, no. 1, pp. 1–10, 2019, doi: 10.1038/s42005-019-0117-9.

[2] N. Sezer and M. Koç, "A comprehensive review on the state-of-the-art of piezoelectric energy harvesting," *Nano Energy*, vol. 80, no. November 2020, p. 105567, 2021, doi: 10.1016/j.nanoen.2020.105567.

[3] E. D. Wheatcroft, A. Pirrera, R. M. J. Groh, J. Shen, and M. Schenk, "Function from Sequential, Interacting Structural Instabilities," 2022.

[4] S. Roundy, "Energy Harvesting for Tire Pressure Monitoring Systems," *Proc. PowerMEMS 2008*, pp. 2–7, 2008.

[5] X. Ma and S. Zhou, "A review of flow-induced vibration energy harvesters," *Energy Convers. Manag.*, vol. 254, no. January, p. 115223, 2022, doi: 10.1016/j.enconman.2022.115223.

[6] R. Elfrink *et al.*, "First autonomous wireless sensor node powered by a vacuum-packaged piezoelectric MEMS energy harvester," pp. 543–546, 2009.

[7] J. Zhang and L. Qin, "A tunable frequency up-conversion wideband piezoelectric vibration energy harvester for low-frequency variable environment using a novel impact- and rope-driven hybrid mechanism," *Appl. Energy*, vol. 240, no. January, pp. 26–34, 2019, doi: 10.1016/j.apenergy.2019.01.261.

[8] J. Pan, W. Qin, and W. Deng, "Promote efficiency of harvesting vibration energy by tailoring potential energy with addition of magnets Promote efficiency of harvesting vibration energy by tailoring potential energy with addition of magnets," vol. 075323, no. July, 2019, doi: 10.1063/1.5114891.

[9] Y. H. Shin *et al.*, "Automatic resonance tuning mechanism for ultra-wide bandwidth mechanical energy harvesting," *Nano Energy*, vol. 77, 2020, doi: 10.1016/j.nanoen.2020.104986.

[10] K. Mohamed, H. Elgamal, and S. A. Kouritem, "An experimental validation of a new shape optimization technique for piezoelectric harvesting cantilever beams," *Alexandria Eng. J.*, vol. 60, no. 1, pp. 1751–1766, 2021, doi: 10.1016/j.aej.2020.11.024.

[11] Y. Jian, L. Tang, G. Hu, Z. Li, and K. C. Aw, "Design of graded piezoelectric metamaterial beam with spatial variation of electrodes," *Int. J. Mech. Sci.*, vol. 218, no. October 2021, p. 107068, 2022, doi: 10.1016/j.ijmecsci.2022.107068.

[12] F. H. Syed, L. W. T. B, and Y. K. Chan, *Proceedings of the Multimedia University Engineering Conference (MECON 2022)*. Atlantis Press International BV, 2023.

[13] M. Safaei and H. A. Sodano, "A review of energy harvesting using piezoelectric materials : state-of-the-art a decade later (2008 – 2018)," 2019.

[14] L. Wang *et al.*, "of bimorph cantilever for piezoelectric vibration," vol. 095067, no. December 2019, 2021, doi: 10.1063/1.5119328.

[15] M. K. Stoj, M. R. Kosanovi, and L. R. Golubovi, "Power Management and Energy Harvesting Techniques for Wireless Sensor Nodes," 2009, doi: 10.1109/TELSKS.2009.5339410.

[16] S. A. Kouritem, M. A. Al-Moghazy, M. Noori, and W. A. Altabey, "Mass tuning technique for a broadband piezoelectric energy harvester array," *Mech. Syst. Signal Process.*, vol. 181, no. May, p. 109500, 2022, doi: 10.1016/j.ymssp.2022.109500.

[17] H. Fu and E. M. Yeatman, "A methodology for low-speed broadband rotational energy harvesting using piezoelectric transduction and frequency up-conversion," *Energy*, vol. 125, pp. 152–161, 2017, doi: 10.1016/j.energy.2017.02.115.